Multistate luminescent solar concentrator 'smart' windows

ADVANCED ENERGY MATERIALS
www.advenergymat.de

Multistate Luminescent Solar Concentrator "Smart" Windows

*Jeroen A. H. P. Sol, Gilles H. Timmermans, Abraham J. van Breugel, Albertus P. H. J. Schenning, and Michael G. Debije**

A supertwist liquid crystalline luminescent solar concentrator (LSC) "smart" window is fabricated which can be switched electrically between three states: one designed for increased light absorption and electrical generation (the "dark" state), one for transparency (the "light" state), and one for enhanced haziness ("scattering" state). In the scattering state, the absorption and edge emissions decrease while the face emissions are enhanced. This new LSC "smart" window state can find application as a privacy feature in housing, but could also allow for a new "smart" window application as a diffuse glazing to increase plant growth in horticultural applications.

1. Introduction

The luminescent solar concentrator, or LSC, has been proposed as an alternative source of electricity generation from sunlight.[1–4] Traditionally in LSCs, luminescent molecules embedded in a polymer plate absorb sunlight: these molecules subsequently emit downshifted light which is trapped in the polymer lightguide by total internal reflection. The emitted light can only escape from the lightguide's edges, where attached photovoltaic (PV) cells convert this light into electricity.

The vast majority of LSCs described to date are static. However, the concept of a liquid crystal (LC)-based switchable LSC window has previously been described.[5–7] These windows demonstrated switching between transparent *on* states, and darker *off* states; part of the incident light is absorbed by the embedded dyes and emitted downshifted, becoming trapped and guided to the edges of the window where the emitted light is converted into electricity. These "smart" windows gave advantages over other LC-based "window" devices[8] and thermo-, photo-, or electrochromic solutions[9] in that they simultaneously offered adjustable spectral and irradiance control of incident sunlight, helping maintain both interior room illumination and regulate temperature, as well as potentially generating power from the redirected sunlight energy.

It is the goal of this work to enhance the applicability of the "smart" LC-based windows by adding a third, "privacy" state to the device. Nonelectricity-generating commercial windows employing LCs with a scattering state have been described.[10] Another device, polymer dispersed liquid crystal (PDLC)-based windows,[8,9,11,12] has found application as scattering panels for use as "privacy state" windows, and electricity generating PDLC type windows have recently been described which display increased angular dependence in the transparent state.[13,14]

By using supertwisted nematic (STN) LC cells,[15–19] one can not only provide this third, "privacy," window state, but also overcome one of the disadvantages of the standard planar LC alignment cells which is the limitation of possible absorbance of incoming light.[5] STN cells present a more complete coverage of possible dye alignment directions through the cell depth, and prevent rotation of the polarization state of incident light, allowing for overall higher light absorption. One necessarily pays for this benefit in that emission light is no longer predominantly directed toward two of four edges as in the planar alignment,[20] but more equally to all sides, requiring more PV cells to cover the entire perimeter.

The switchable STN LSC window could find application not only in places of human work and habitation but also in horticulture, specifically in the area of protected cultivation in greenhouses.[21] Greenhouses are designed to provide optimal growth conditions for plants through controlling temperature, CO_2 concentration, humidity, and light. In northern latitudes it is commonly held that 1% extra light in the photosynthetic active (PAR) region of the spectrum results in 0.5–1% more yield,[22] and in addition to light intensity, both spectral[23] and geometrical distributions[24] of the light are important factors in plant and fruit production. By increasing the haziness of the greenhouse cover, there is increased diffuseness of light, allowing light to penetrate deeper into the plant canopy and reach the lower leaves, resulting in an increase in production[25,26] and prevention of leaf burning.[27,28] Currently, this is done by covering the greenhouse with whitewash or a shadow screen, among other techniques.[29,30]

J. A. H. P. Sol, G. H. Timmermans, Prof. A. P. H. J. Schenning, Dr. M. G. Debije
Chemical Engineering & Chemistry
Functional Organic Materials and Devices
Eindhoven University of Technology
5600 MB, Eindhoven, The Netherlands
E-mail: m.g.debije@tue.nl
A. J. van Breugel
Wageningen Plant Research
Greenhouse Horticulture
Wageningen University and Research
6708 PB, Wageningen, The Netherlands
Prof. A. P. H. J. Schenning
Institute for Complex Molecular Systems
Eindhoven University of Technology
5600 MB, Eindhoven, The Netherlands

DOI: 10.1002/aenm.201702922

We describe a new LSC-type window that uses a fluorescent dye embedded in an LC cell with supertwist alignment. This cell configuration allows more complete absorption of the incident light, and thus a darker *off* state, as well as allow for a third, scattering state, which could find use as privacy glass in places of human habitation, or as diffusive glazing in greenhouses to improve plant growth.

2. Results and Discussion

2.1. "Smart" Windows for Electricity Generation

In a regular twisted nematic display panel, the LC cell alignment layers are rotated by 90°, resulting in a 90° twist in the LC molecular director over the depth of the cell.[31] In the Mauguin regime, incident polarized light will rotate and follow the LC director when[32]

$$\Delta n d > \frac{\phi\lambda}{\pi} \tag{1}$$

where Δn is the difference between the extraordinary and ordinary refractive indexes of the LC, d is the cell gap in µm, ϕ (rad) is the total twist of LC director across the cell, and λ is the wavelength in µm (the Mauguin regime). By creating a tight enough rotation of the LC director across the cell, the "supertwisted" LC ensures that light cannot follow the rotating LC, and this results in all polarizations being available to be absorbed by the embedded dye molecules. We create the supertwist across the cell thickness by adding a chiral dopant to the LC mixture.[33] The pitch length p (µm) of the twist is dependent on the weight fraction of the chiral dopant, c, and can be calculated by

$$p = (\beta c)^{-1} \tag{2}$$

where β (μm^{-1}) is the helical twisting power (HTP) of the chiral dopant. The total rotation of the LC director across the depth of the cell can be calculated by

Table 1. List of E7 filled LSC cells and their composition.

ID	Dye	wt%	S-811 [wt%]
Yell25	K160	0.25	–
Yell25c		0.25	3.4
Red25	Red 305	0.25	–
Red25c		0.25	3.4

$$\phi = 2\pi d\beta c \tag{3}$$

Equations (1) and (3) can be simplified to Equation (4). If the condition is met, the Mauguin regime is relevant.

$$\Delta n > 2\lambda\beta c \tag{4}$$

A cell containing 0.25 wt% K160 dye and 3.42 wt% S-811 chiral dopant (HTP = –11 μm^{-1}) in nematic LC mix E7 was produced (Yell25c: see **Table 1** for definitions of all fluorescent dye/LC systems used in this text). K160 is a coumarin-based dye chosen for its solubility and good alignment in the LC host, and its proven performance in LSC-based window devices.[5] The number of pitches in the cell was calculated to be 7.08, as such the incident light will not be able to follow the cell "twist." The resultant *apparent macroscopic order parameter* of the embedded dye, S_{apparent}, defined as

$$S_{\text{apparent}} = \frac{A_{\text{par}} - A_{\text{per}}}{A_{\text{par}} + 2A_{\text{per}}} \tag{5}$$

where A_{par} and A_{per} are the absorbance of the cells with light polarized parallel and perpendicular to the alignment direction of the cell, respectively, was found to be 0.16. For reference, the K160 dye in a pure planar cell or polymerized LC film has an order parameter around 0.5.[5,20] It should be noted that locally, order between the dye and LC host is maintained, but as the dye shows rotational alignment throughout the cell depth, a lower macroscopic order parameter is found.

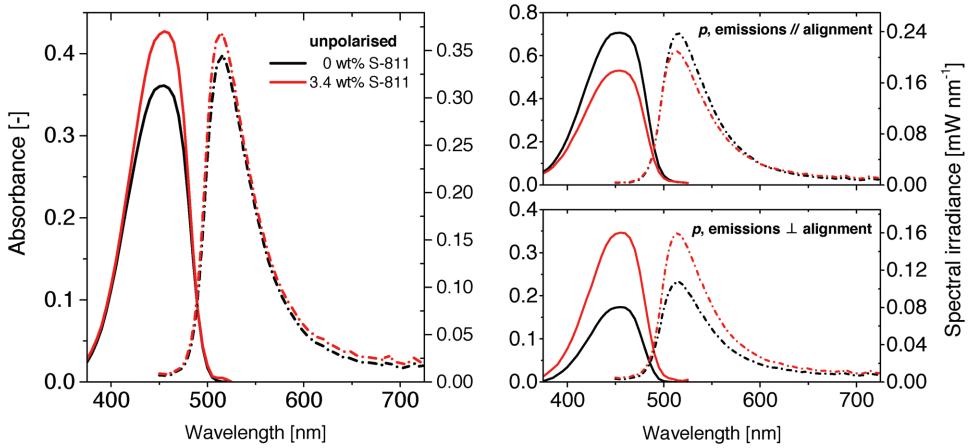

Figure 1. Absorbance (solid lines) and edge emission (dashed lines) spectra of 20 µm gap cells containing 0.25% K160 dye and either 0 wt% (black lines) or 3.4 wt% (red lines) of chiral dopant S-811 in host LC E7 measured with (left) unpolarized light; (top right) light polarized parallel to the alignment direction; and (bottom right) light polarized perpendicular to the alignment direction.

The absorbance and the total edge emission of the devices with and without chiral dopant at rest, exposed to both polarized and unpolarized light are seen in **Figure 1**. Comparing the absorption characteristics of the LSCs confirms that the chiral doped STN cell has indeed captured 10% more of the unpolarized incident light than the planar cell, with 11% more power emitted from the edges. The fraction of incident light energy absorbed (between 400 and 491 nm) by both planar (Yell25) and STN cells with 0.25 wt% K160 dye (Yell25c) as a function of applied voltage was calculated from transmission spectra as described in the Experimental Section, and are shown in **Figure 2**. The planar cell performs similarly to cells described in the earlier work on LSC smart windows.[5] The LCs transition gradually from a planar orientation to a homeotropic state upon increasing the voltage, resulting in a concomitant decrease in light absorption as the dye absorption dipole is eventually oriented homeotropically (perpendicular to the lightguide surface), and thus is least efficient at absorbing light.

At low voltages (<5 V_{RMS}, the root mean squared applied potential), a dark, colored state is observable; under magnification, chiral nematic (cholesteric) defect lines in the STN cells are visible (polarized optical microscopy images taken with the same sample between crossed polarizers are given as Figure S1 in the Supporting Information). Upon applying higher electric potentials, two additional states can be observed. Intermediate voltages (≈5–15 V_{RMS}) reveal a strongly scattering state, likely focal conic.[34] Finally, higher voltages (>15 V_{RMS}) align the LCs and dye homeotropically, rendering the sample nearly colorless: images of the STN cell in all three states are shown in Figure 2 and Figure S1 in the Supporting Information for the Yell25c sample at 0, 10, and 28 V_{RMS}, respectively.

At 0 V_{RMS}, the increased absorption in the STN cell compared to the planar cell is due to the "twisted" arrangement of the K160 dye. Absorption decreases at intermediate voltages when the system is in the scattering state, but there is less of a drop than seen in the planar system at equivalent voltage. At higher voltages, the LC reorients to the homeotropic state, and the resulting transmission and surface emissions become identical to that of the planar cells with the same amount of chiral dopant (see Figure 2 and Figure S2 in the Supporting Information for the transmission spectra of the three states).

The total edge emissions of fluorescent light integrated over the wavelength region of 350–850 nm from the cells exposed to light from a solar simulator were measured at the various applied voltages using an integrating sphere, and are shown in **Table 2**. An example comparison of the integrated edge emissions can be seen in **Figure 3** for the Yell25 planar and the Yell25c cells. For both cells, the edge emissions are highest at 0 V_{RMS} and quickly drop with increasing voltages. After the initial drop, the Yell25 cell shows a slow continuous decrease while the Yell25c forms a plateau at the scattering state around 10 V_{RMS}. After 17 V_{RMS} the emissions are similar to those of the planar cell.

Edge emissions data show generally the same trend as the absorption data; that is, at increasing voltage—and consequent lowering absorption—integrated edge emissions from the LSC decline. The ratio of outputs between strong and weak emitting edges decreases as the electric field's strength over the LC cell is increased (see Table 2). In the planar state, the emission of

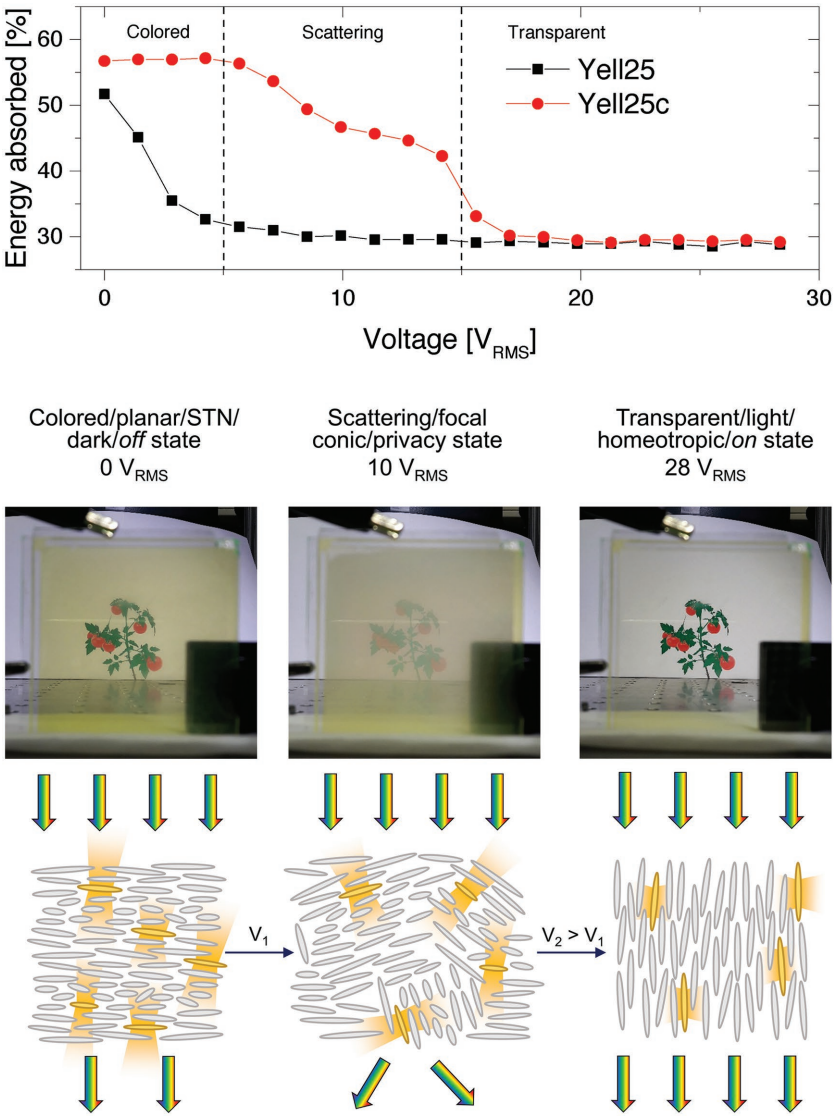

Figure 2. (Top) Calculated fractional absorbance of the incident solar simulator light by the LC/dye systems as a function of applied voltage for 0.25 wt% of the K160 dye (integrated from 400 to 491 nm). Dashed vertical lines indicate state changes for the STN cells. (Middle) Photographs of the Yell25c cell at (left) 0 V_{RMS}, (middle) 10 V_{RMS}, and (right) 28 V_{RMS}. (Bottom) Schematic representation of the alignment of the LCs, dyes, and the emission direction. A video of this switching action may be found in the Supporting Information.

Table 2. Measured edge emissions from the 5 × 5 cm^2 cells, calculated ratio between emission of strong/weak edge, and optical conversion and internal efficiencies for the various samples.

Sample	Edge emission [mW][a)]			Ratio strong/weak edge			Optical conversion efficiency [%][3,37,38]			Internal efficiency [%][39]		
	0 V_{RMS}	10 V_{RMS}	28 V_{RMS}	0 V_{RMS}	10 V_{RMS}	28 V_{RMS}	0 V_{RMS}	10 V_{RMS}	28 V_{RMS}	0 V_{RMS}	10 V_{RMS}	28 V_{RMS}
Yell25	33	26	25	1.2	1.0	1.0	3.3	2.6	2.5	47	61	60
Yell25c	38	30	26	1.0	1.0	1.0	3.8	3.0	2.6	48	45	63

[a)]Edge emission over all four sides, obtained by doubling the sum of emissions from the parallel and perpendicular cell edges integrated 350–850 nm.

the dye molecules is predominantly from the lightguide top and bottom (considered losses) and from the edges parallel to the alignment direction.[20] In the homeotropic state, the molecules orient so that the emission is distributed equally toward the four edges with little light directed toward the top or bottom surfaces.[35,36]

The *optical conversion efficiency*,[3,37,38] defined by

$$\eta_{opt} = \frac{P_{out}}{P_{in}} \tag{6}$$

where P_{out} (W) is the optical power emitted over all four edges for the wavelength range of 350–850 nm, and P_{in} (W) is the incoming optical power over the surface of the sample in the same wavelength range. Our calculated optical efficiencies (see **Table 3**) compare favorably with previous work,[3] although it must be noted we only are capable of measuring a limited spectral range for the incident light: we estimate the efficiencies we would obtain for the spectrum out to 1400 nm would be decreased ≈30%.

Internal efficiency (η_{int}) describes the fraction of photons exiting the device from the edges per photon absorbed through the top surface.[39] Calculations are done using

$$\eta_{int} = \frac{\text{photon flow out of edges}}{\text{photon flow absorbed}} = \frac{\int_{emission} P_{out}(\lambda_{em}) \frac{\lambda_{em}}{hc} d\lambda_{em}}{\int_{absorption} P'_{in}(\lambda_{abs}) \frac{\lambda_{abs}}{hc} A(\lambda) d\lambda_{abs}} \tag{7}$$

where "emission" and "absorption" represent the dye-dependent wavelength ranges for absorption and emission (400–491 and 492–640 nm), h is Planck's constant (in J s), and c the speed of light (in m s^{-1}). $P'_{in}(\lambda)$ is the incoming power spectrum (after subtracting reflection measured from a pure E7-filled cell: 15 ± 3%). In planar and STN cells, the highest internal efficiency is found when switched to the homeotropic state: the absorption decreases (see Figure 2), while, concomitantly, the emission transition dipole orients in such a way that more emitted photons are captured in the lightguide. Measured edge emission efficiency values compare reasonably well with those reported previously (see Table 1).[5]

For window applications, it is necessary to consider the effect the window has on the view experienced by the user, not only along direct but also indirect sightlines. In **Figure 4** we show photographs of the Yell25c cell in three states, viewing a background image oriented both normal to the cell, and with the "window" at roughly a 45° angle. In PDLC-based power generating "window" elements, there is considerably more image haziness at oblique viewing angles,[13] which could render the STN LC-based window preferable for use in situations where distinct external views are desired under all viewing angles. Similarly, dual-layer windows have been described using a PDLC backing for an LSC lightguide.[14] This latter window suffers from permanent coloration. One could argue such a system could be improved by coupling a rear-side PDLC window with a switchable LSC[5]; however, the STN device presented here provides the three window states (*on*, *off*, and scattering) in a single cell, simplifying manufacture and deployment.

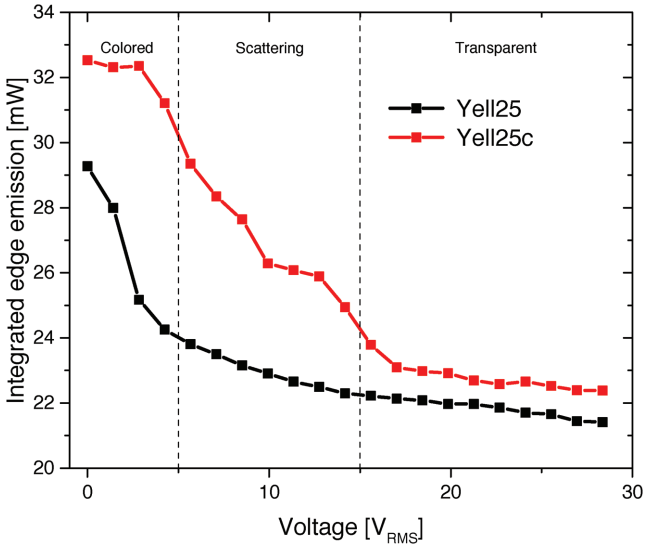

Figure 3. Total integrated edge emission from 350 to 850 nm of the planar Yell25 (black) and STN Yell25c (red) samples as a function of applied voltage. Dashed vertical lines indicate state changes for the STN cells.

2.2. "Smart" Glazing for Greenhouses

Both the haze and the lightguide surface emissions of the STN cells were examined in more detail for possible application in a greenhouse architecture (depicted in Figure S3 in the Supporting Information). In the colored *off* state, the cell absorbs incident sunlight and converts this to a longer wavelength to be redirected toward the lightguide edge, where it could either be used to generate electricity via an attached PV cell, or further guided to illuminate the crop lower in the canopy where light is more scarce.[40] In the focal conic, scattering state, light is more likely scattered through the top and bottom surfaces, resulting

Table 3. Measured average transmission in PAR (400–700 nm), haze factor, and the energy absorbed and emitted in region 1 and region 2.

Sample	Perpendicular transmission in PAR [%]			Haze factor [%] (±5%)			Energy absorbed Region 1 [%][a)]			Energy emitted Region 2 [%][b)]		
	0 V_{RMS}	10 V_{RMS}	28 V_{RMS}	0 V_{RMS}	10 V_{RMS}	28 V_{RMS}	0 V_{RMS}	10 V_{RMS}	28 V_{RMS}	0 V_{RMS}	10 V_{RMS}	28 V_{RMS}
Yell25	75	78	79	4	4	4	52	30	29	5.5	3.9	4.1
Yell25c	70	69	75	6	66	5	57	47	29	5.7	5.8	3.4
Red25	78	77	77	7	8	8	14	15	15	4.4	4.7	5.3
Red25c	75	73	75	7	65	5	13	14	15	4.9	6.2	5.2

[a)]Region 1 represents 400–491 nm (K160) or 400–606 nm (Red 305); [b)]Region 2 represents 492–700 nm (K160) or 607–700 nm (Red 305).

in additional downshifted light entering the greenhouse, while all other, nonabsorbed incident wavelengths are simply scattered, allowing more indirect illumination of the plants. Finally, in the homeotropic, *on* state, the cell does not interfere with the incident light and acts like a standard window.

The energy of the absorbed incident light of the Yell25c STN system at 0 V_{RMS} was estimated to be 57% of light between 400 and 491 nm, while 5.7% is added to the bottom face output by fluorescence between 492 and 700 nm (after correcting for Fresnel reflection by the LC cell, which was measured by comparing the transmitted spectrum of an E7 filled cell with the unimpeded solar simulator spectrum; see Figure S4 in the Supporting Information). At 28 V_{RMS}, in which the absorption cross-section is smallest and the window is most transparent, these numbers are 29% and 3.4%, respectively, and for the scattering state at 10 V_{RMS}, 47% and 5.8%.

To make the window more active within the photosynthetically active radiation (PAR, 400–700 nm) region most relevant for plant growth, we made cells containing the ubiquitous fluorescent dye Lumogen F Red 305 from BASF, a very common dye used in LSC applications (see Table 1).[21,41–45] The additional light leaving the surface of the cells containing K160 dye (integrated from 492 to 700 nm) as a function of applied voltage are shown in **Figure 5**a, and of the Red 305 dye (integrated from 607 to 700 nm) in Figure 5b.

The surface emissions of the K160 planar samples decrease with LC/dye reorientation to homeotropic, since the emission axis is such that more light is directed into the light guiding mode of the LSC cell, and less light is coupled out on the surface, as seen previously.[46–48] For the STN K160 system, the surface emission shows a considerable increase when the window is in the scattering state. This is a result of the increased randomization of the light originally emitted into the cone of total internal reflection for the lightguides, leading to the scatter of the light into the escape modes of the lightguide. At higher voltages, the LC reorients to the homeotropic state, and the resulting surface emissions become identical to that of the planar cells with the same amount of chiral dopant. The

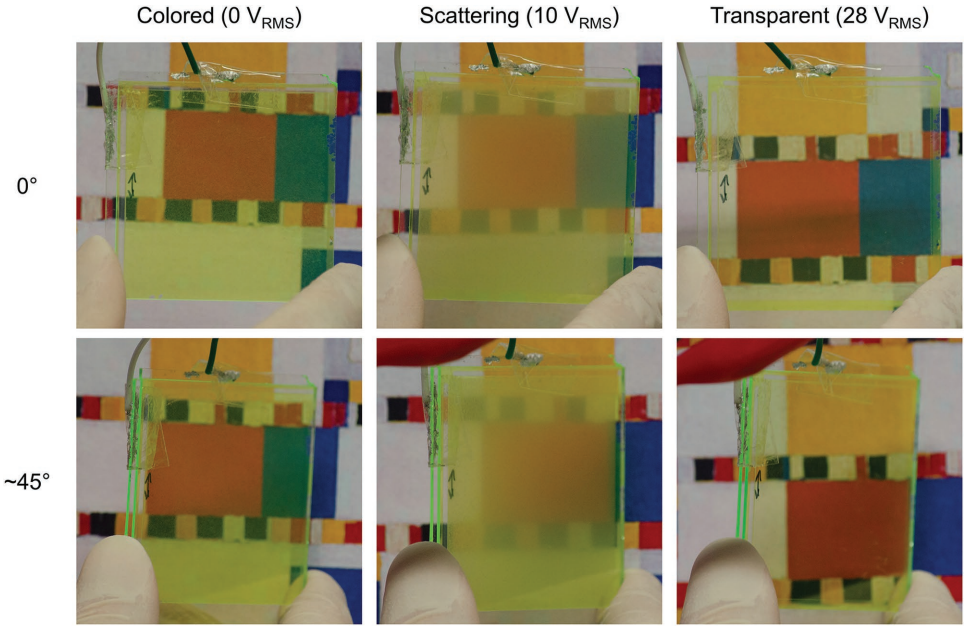

Figure 4. Photographs of Yell25c cell in the STN (0 V_{RMS}, left), focal conic, scattering (10 V_{RMS}, center), and homeotropic (28 V_{RMS}, right) states when the device is oriented normal (top row) or at an oblique angle (bottom row) to a distant visual. Note the brightly emitting edges visible in the bottom row of photographs.

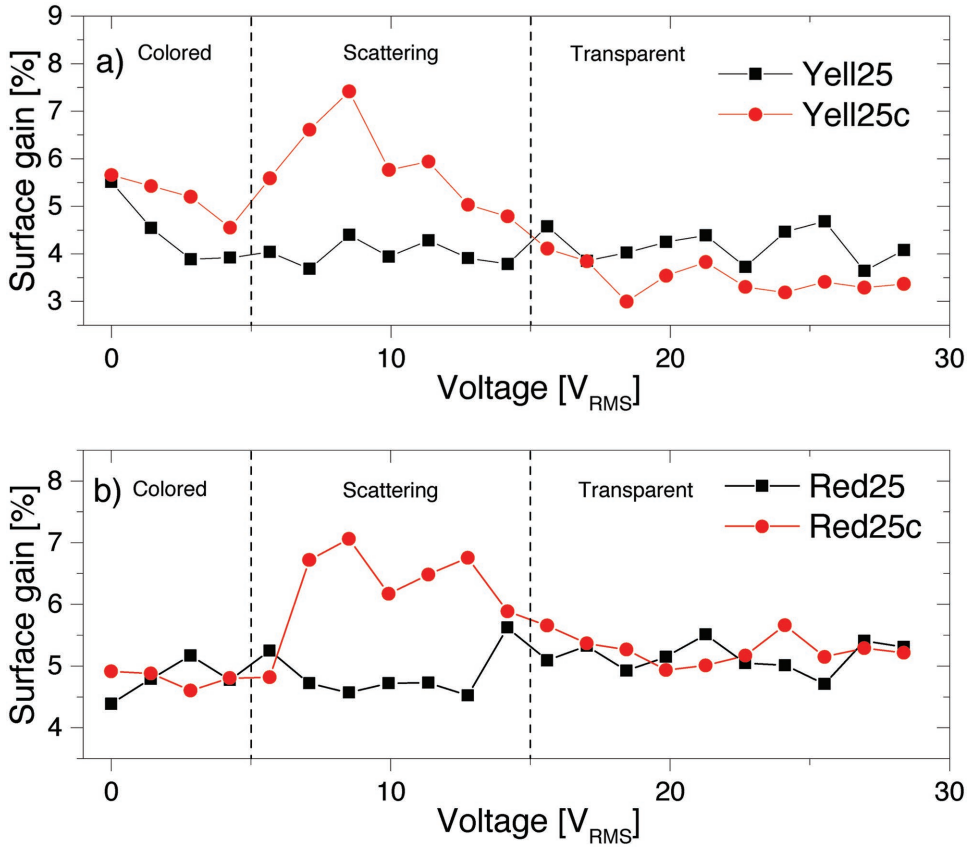

Figure 5. Change in surface emission for STN cells exposed to light from a solar simulator as a function of applied voltage for a) K160 integrated from 492 to 700 nm and b) Red 305 integrated from 607 to 700 nm.

scattering state is also effective at redirecting the emission light out of the lightguide for the Red 305 containing STN cells (see Table 3).

The average transmission in the PAR is given in Table 3. For maximizing the amount of light reaching the crop, the homeotropic (28 V_{RMS}) state is optimal. The color of the light reaching the crop is affected by the change in the amount of light absorbed and emitted by the dyes. In Table 3 this change is shown compared to the normal solar spectrum for the absorption in Region 1 (400–491 nm for the K160 dye and 400–606 nm for the Red 305 dye) and the emission in Region 2 (492–700 nm for the K160 dye or 607–700 nm for the Red 305 dye).

As mentioned in the Introduction, hazy glazing has considerable impact on plant growth in greenhouses. For instance, tomatoes grown under a greenhouse cover with a haze factor of 71% show a 7.2% increase of cumulative crop synthesis over a complete growing cycle compared to standard float glass of similar hemispherical PAR transmittance.[25] Because of this, the haze for each STN cell was characterized, and the results are displayed in **Figure 6** and Table 3. It is obvious there is no significant change in the haze value in the planar Yell25 cell, which remained at 4% in all cases. In contrast, the STN Yell25c cell demonstrated a significant increase of haze from 6% in the *off* state to 66% at 10 V_{RMS}, and with a significant angular spread. Again, this haze decreased to 5% in the homeotropic state at 28 V_{RMS}. In general, the haze from the Red 305 cells are higher, partially a result of its lower order parameter in the host LC.[5]

Advanced greenhouses use glass manufactured specifically to generate haze, with haze values ranging from 20 to 100%; "medium" diffusion is described as being around 40%, and "high" diffusion characterized for haze values around 80% or greater.[49] Thus, the nonoptimized scattering states of the windows described in this work approach the "high" haze seen in existing greenhouse glass, with the additional capability of switching to the low haze state, which is not possible in the textured glass solutions. The 4–7% haze in the "clear" state compares favorably to traditional clear greenhouse glass.[49]

All of the critical crop-growth features of greenhouse glass (transmission, haziness, and color) could be regulated by the use of the dye-doped STN "smart" window, which could both augment food production and diminish energy usage.[21,50] In particular, the additional scattering state achieved at relatively low voltages (5–15 V_{RMS}) could be of considerable interest. This scattering state is able to geometrically disperse light with enhanced surface outcoupling due to the scattering focal conic structures. However, the haze comes at the cost of total light transmission, so would be less appropriate for use in winter, for instance, when light is naturally more diffuse due to atmospheric conditions.[24] In such cases, it would be beneficial to switch the window to the transparent homeotropic state to maximize total light transmission. In intermediate cases, the STN

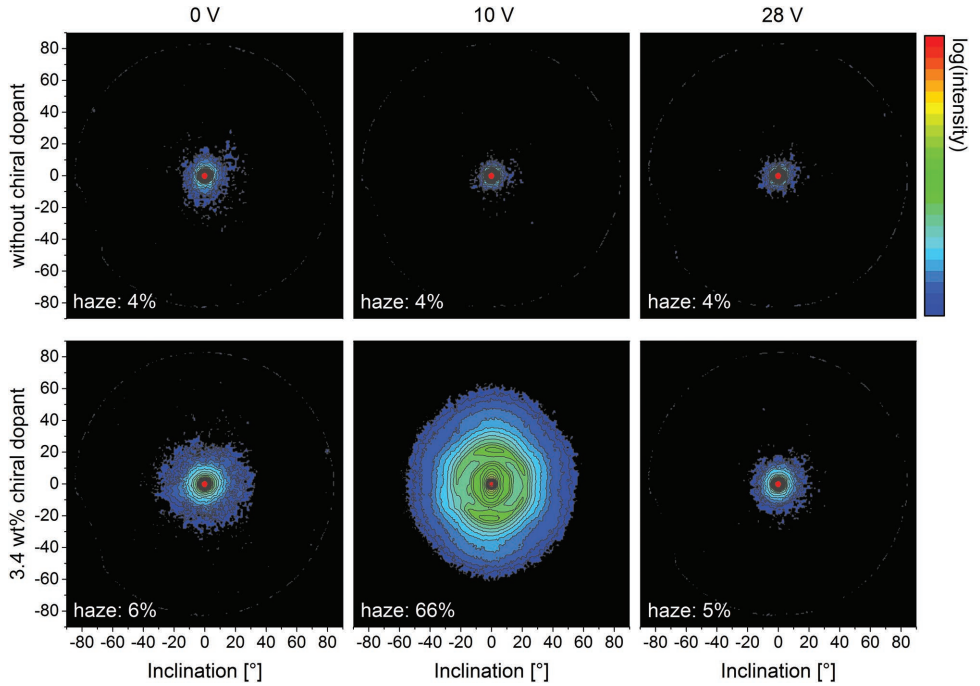

Figure 6. Haze measurements of the Yell25 sample (top) and Yell25c sample (bottom) showing the intensity and the angle of the light being scattered (left) 0 V_{RMS}, (middle) 10 V_{RMS}, and (right) 28 V_{RMS}.

state could reduce total light intensity on the plants, enhance red illumination, with the excess red light used to generate electricity for other local use purposes, or directed into a fiber to allow for lower canopy illumination of the plants to enhance growth.

Systems based on the STN LSC "smart" windows could be tailored to fit the needs of the greenhouse by incorporating a luminophore with matching absorption and luminescence characteristics to the crop requirements. To retain maximum light transmission in the PAR region, a large Stokes shift dye would be ideal. Such a dye should absorb in the ultraviolet region and convert this to surplus radiation useful for photosynthesis.

3. Conclusion

This work shows that adding a chiral dopant to a planar aligned cell results in a supertwist alignment which demonstrates increased absorption and emission compared to the standard "planar" window design. The STN cell displays a third, scattering state at intermediate voltages which complements the standard "dark" and "light" states of the LSC "smart" window. The increased face emission in the scattering state is accompanied by a decrease in edge emissions. By applying different voltages to the device, the transmitted spectra, haze, and intensity can be directly regulated. This is not only useful for offices and homes but highly desirable in high-tech greenhouses. Additionally—but not unimportantly—it is possible to simultaneously use the lightguide edge emissions for photovoltaic power generation.

4. Experimental Section

Commercial 10 × 10 mm^2 switching area, 19 µm gap cells were purchased from Instec Inc. (SG100A200VG180). Custom-made cells (about 50 × 50 mm^2 switching area, 20 µm spacing) from LC-Tec Displays AB were also purchased.

Either DFSB-K160 (Risk Reactor Inc.) or Lumogen F Red 305 (BASF SE) dye was dissolved in the nematic LC mix E7 (Merck KGaA) in a 0.25 wt% concentration. "Supertwist" mixtures were prepared by adding 3.4 wt% of left-handed chiral dopant S-811 (Merck) to the LC/dye mixtures, which were introduced into the cells via capillary filling. Table 1 depicts the combinations of dyes and LCs used.

UV–vis absorption measurements were done using a Perkin Elmer Lambda 750 equipped with an integrating sphere detector. Microscopic images were recorded with a Leica DM6000 M polarized microscope. LSC edge emissions (over the 5 × 0.2 cm^2 edge area) and surface transmissions (through a 2.5 × 2.5 cm^2 area) were recorded with a Labsphere SLMS 1050 integrating sphere connected to an International Light RPS900 diode array detector. Illumination for emission measurements was provided by a 300 W Lot-Oriel solar simulator equipped with filters to emulate the AM1.5 solar spectrum located at a distance of approximately 15 cm above the sample, using a black (absorbing) background. Integrated power from the lamp (350–850 nm) was 720 ± 40 mW over the surface of the sample. The light of the lamp was slightly polarized with an ≈10% bias along the axis perpendicular to the opening of the integrating sphere: the results reported in this work have not been corrected for this bias as in the previous work[5] as the variety of LC alignments renders correlation of LC alignments and polarizations ambiguous. Total edge emission described in this work was derived by doubling the sum of the output of two orthogonal cell edges (effectively calculating the would-be emission from all four edges combined), since due to the LC and dye alignment, spectral outputs from the orthogonal edges differ.[20]

The energy of the absorbed incident light can be calculated by determining the wavelength-dependent quantity of light removed from the incident solar simulator spectrum as it enters an integrating sphere

through the STN cell (corrected for measured reflection by a pure E7 filled cell), and integrating over the appropriate wavelength ranges; likewise, the emission from the surface can be determined from the quantity of additional light entering the sphere from the rear surface of the illuminated cell determined in the same manner as previously described.[51]

Sine wave voltage modulation at 1000 Hz was applied to the cells using a laboratory function generator (Agilent 33220A) coupled to a 20 × voltage amplifier (FLC Electronics F20A) in the range of 0–30 V_{RMS}.

The haze of the samples was measured using a Radiant Zemax IS-SA, using a procedure described by Hemming et al.[49] In short, a coherent beam of light from a halogen light source was directed through the sample. The transmitted light was scattered onto a semisphere, and a bidirectional transmittance distribution function was measured using a light intensity camera placed underneath. The resulting angular energy distribution was subsequently used to calculate the haze value by integrating from 2.5° to 90° (diffuse light, with 2.5° the critical angle according to ASTM-D1003-13) and dividing this value by integrating the angular energy distribution from 0° to 90° (specular light).

Supporting Information

Supporting Information is available from the Wiley Online Library or from the author.

Acknowledgements

The authors would like to acknowledge the support of the TKI PPS Smart Materials for Greenhouses program for their support of this work. On April 25th, 2018 a number of changes were made to the article. The name D. K. G. De Boer in reference 43 was changed to D. K. G. de Boer. The name A. J. Van Breugel in reference 49 was changed to A. J. van Breugel. The expression $P'_n(\lambda)$ on page 4 was changed to $P'_{in}(\lambda)$.

Conflict of Interest

The authors declare no conflict of interest.

Keywords

fluorescence, luminescent solar concentrators, smart windows, supertwist nematic liquid crystals

Received: October 20, 2017
Revised: November 15, 2017
Published online: January 22, 2018

[1] W. H. Weber, J. Lambe, *Appl. Opt.* **1976**, *15*, 2299.
[2] A. Goetzberger, W. Greubel, *Appl. Phys.* **1977**, *14*, 123.
[3] B. McKenna, R. C. Evans, *Adv. Mater.* **2017**, *29*, 1606491.
[4] M. G. Debije, P. P. C. Verbunt, *Adv. Energy Mater.* **2012**, *2*, 12.
[5] M. G. Debije, *Adv. Funct. Mater.* **2010**, *20*, 1498.
[6] A. M. Kendhale, A. P. H. J. Schenning, M. G. Debije, *J. Mater. Chem. A* **2013**, *1*, 229.
[7] R. W. MacQueen, Y. Y. Cheng, R. G. C. R. Clady, T. W. Schmidt, *Opt. Express* **2010**, *18*, A161.
[8] S. Sato, M. M. Labes, *J. Appl. Phys.* **1981**, *3941*, 3941.
[9] Y. Wang, E. L. Runnerstom, D. J. Milliron, *Annu. Rev. Chem. Biomol. Eng.* **2016**, *7*, 1.
[10] C. L. van Oosten, *Device for the regulation of light transmission* **2017**, WO2017008881A1.
[11] S. Bronnikov, S. Kostromin, V. Zuev, *J. Macromol. Sci. Part B* **2013**, *52*, 1718.
[12] F. Ahmad, M. Jamil, Y. J. Jeon, *Electron. Mater. Lett.* **2014**, *10*, 679.
[13] J. Murray, J. N. Munday, *ACS Photonics* **2017**, *4*, 1.
[14] F. Mateen, H. Oh, W. Jung, S. Y. Lee, H. Kikuchi, S. K. Hong, *Liq. Cryst.* **2017**, 1.
[15] S. C. Guy, *Displays* **1993**, *14*, 32.
[16] F. Leenhouts, M. Schadt, H. Roche, *J. Appl. Phys.* **1986**, *60*, 3275.
[17] T. J. Scheffer, J. Nehring, *J. Appl. Phys.* **1985**, *58*, 3022.
[18] K.-H. Kim, H.-J. Jin, K.-H. Park, J.-H. Lee, J. C. Kim, T.-H. Yoon, *Opt. Express* **2010**, *18*, 16745.
[19] J.-W. Huh, B.-H. Yu, J. Heo, T.-H. Yoon, *Appl. Opt.* **2015**, *54*, 3792.
[20] P. P. C. Verbunt, A. Kaiser, K. Hermans, C. W. M. Bastiaansen, D. J. Broer, M. G. Debije, *Adv. Funct. Mater.* **2009**, *19*, 2714.
[21] C. Corrado, S. W. Leow, M. Osborn, I. Carbone, K. Hellier, M. Short, G. Alers, S. A. Carter, *J. Renewable Sustainable Energy* **2016**, *8*, 1.
[22] L. F. M. Marcelis, A. G. M. Broekhuijsen, E. Meinen, E. M. F. M. Nijs, M. G. M. Raaphorst, *Acta Hortic.* **2006**, *711*, 97.
[23] W. van Ieperen, *Acta Hortic.* **2012**, *956*, 131.
[24] S. Hemming, V. Mohammadkhani, T. Dueck, *Acta Hortic.* **2008**, *797*, 469.
[25] T. Li, E. Heuvelink, T. A. Dueck, J. Janse, G. Gort, L. F. M. Marcelis, *Ann. Bot.* **2014**, *114*, 145.
[26] S. Hemming, T. A. Dueck, J. Janse, F. van Noort, *Acta Hortic.* **2008**, *801*, 1293.
[27] W. Chirachint, D. W. Turner, *Sci. Hortic. (Amsterdam)* **1988**, *36*, 1.
[28] M. P. N. Gent, *HortScience* **2007**, *42*, 514.
[29] C. Stanghellini, J. Dai, F. Kempkes, *Biosyst. Eng.* **2011**, *110*, 261.
[30] A. Abdel-Ghany, *Jpn. J. Trop. Agric.* **2001**, *45*, 242.
[31] P. W. Benzie, S. J. Elston, in *Handbook of Visual Display Technology* (Eds: J. Chen, W. Cranton, M. Fihn), Springer, Berlin, Heidelberg **2012**.
[32] T. J. Scheffer, J. Nehring, in *Liquid Crystals—Applications and Uses* (Ed.: B. Bahadur), World Scientific, Singapore **1990**.
[33] D. J. Broer, I. Heynderickx, *Macromolecules* **1990**, *23*, 2474.
[34] M. Kawachi, K. Kato, O. Kogure, *Jpn. J. Appl. Phys.* **1978**, *17*, 1245.
[35] P. P. C. Verbunt, C. W. M. Bastiaansen, D. J. Broer, M. G. Debije, in *24th Eur. Photovolt. Sol. Energy Conf.*, **2009**, WIP GmbH & Co-KG, pp. 381–384.
[36] C. L. Mulder, P. D. Reusswig, A. M. Velázquez, H. Kim, C. Rotschild, M. A. Baldo, *Opt. Express* **2010**, *18*, A79.
[37] S. F. H. Correia, P. P. Lima, E. Pecoraro, S. J. L. Ribeiro, P. S. André, R. A. S. Ferreira, L. D. Carlos, *Prog. Photovoltaics Res. Appl.* **2016**, *24*, 1178.
[38] F. Purcell-Milton, Y. K. Gun'ko, *J. Mater. Chem.* **2012**, *22*, 16687.
[39] C. Tummeltshammer, A. Taylor, A. J. Kenyon, I. Papakonstantinou, *Sol. Energy Mater. Sol. Cells* **2016**, *144*, 40.
[40] A. A. Earp, G. B. Smith, J. Franklin, P. D. Swift, *Sol. Energy Mater. Sol. Cells* **2004**, *84*, 411.
[41] G. Seybold, G. Wagenblast, *Dyes Pigm.* **1989**, *11*, 303.
[42] L. H. Slooff, E. E. Bende, A. R. Burgers, T. Budel, M. Pravettoni, R. P. Kenny, E. D. Dunlop, A. Büchtemann, *Phys. Status Solidi R* **2008**, *2*, 257.
[43] L. Desmet, A. J. M. Ras, D. K. G. de Boer, M. G. Debije, *Opt. Lett.* **2012**, *37*, 3087.
[44] L. R. Wilson, B. S. Richards, *Appl. Opt.* **2009**, *48*, 212.
[45] F. M. Vossen, M. P. J. Aarts, M. G. Debije, *Energy Build.* **2016**, *113*, 123.
[46] M. G. Debije, P. P. C. Verbunt, in *Tech. Proc. 2011 NSTI Nanotechnol. Conf. Expo, NSTI-Nanotech 2011*, Vol. *1*, **2011**, NSTI p. 584.
[47] C. L. Mulder, P. D. Reusswig, A. P. Beyler, H. Kim, C. Rotschild, M. A. Baldo, *Opt. Express* **2010**, *18*, A91.
[48] P. P. C. Verbunt, C. Sánchez-Somolinos, D. J. Broer, M. G. Debije, *Opt. Express* **2013**, *21*, A485.
[49] S. Hemming, G. L. A. M. Swinkels, A. J. van Breugel, V. Mohammadkhani, *Acta Hortic.* **2016**, *1134*, 309.
[50] S. Hemming, E. A. van Os, J. Hemming, J. A. Dieleman, *Eur. J. Hortic. Sci.* **2006**, *71*, 145.
[51] M. G. Debije, P. P. C. Verbunt, B. C. Rowan, B. S. Richards, T. Hoeks, *Appl. Opt.* **2008**, *47*, 6763.